HERITABILITY OF BRAIN NETWORK TOPOLOGY IN 853 TWINS AND SIBLINGS

L. Zhan[1, 2], N. Jahanshad[2], J. Faskowitz[2], D. Zhu[2], G. Prasad[2], N.G. Martin[3],
G.I. de Zubicaray[4], K.L. McMahon[5], M.J. Wright[3], P.M. Thompson[2]

1. Dept. of Neurology, University of California, Los Angeles, CA 90095, USA
2. Imaging Genetics Center, Keck School of Medicine,
University of Southern California, Marina Del Rey, CA 90292, USA
3. QIMR Berghofer Medical Research Institute, Brisbane, QLD 4029, Australia
4. School of Psychology, University of Queensland, Brisbane, QLD 4072, Australia
5. Centre for Advanced Imaging, University of Queensland, Brisbane, QLD 4072, Australia

ABSTRACT

Anatomical brain networks change throughout life and with diseases. Genetic analysis of these networks may help identify processes giving rise to heritable brain disorders, but we do not yet know which network measures are promising for genetic analyses. Many factors affect the downstream results, such as the tractography algorithm used to define structural connectivity. We tested nine different tractography algorithms and four normalization methods to compute brain networks for 853 young healthy adults (twins and their siblings). We fitted genetic structural equation models to all nine network measures, after a normalization step to increase network consistency across tractography algorithms. Probabilistic tractography algorithms with global optimization (such as Probtrackx and Hough) yielded higher heritability statistics than "greedy" algorithms (such as FACT) which process small neighborhoods at each step. Some global network measures (probtrackx-derived GLOB and ST) showed significant genetic effects, making them attractive targets for genome-wide association studies.

Index Terms— diffusion MRI, Brain Network, Tractography, ICC, Normalization

1. INTRODUCTION

Diffusion-weighted MRI is a non-invasive technique sensitive to white matter microstructure. Using diffusion MRI, water diffusion in each voxel can be modeled using a tensor or an orientation distribution function (ODF). Dominant diffusion directions may be extracted from these diffusion models; by following neighboring voxels' dominant diffusion directions, large-scale neuronal tracts may be reconstructed. Anatomical brain networks can be modeled by counting the proportion of detected fibers that intersect or interconnect pairs of regions of interest (ROIs), defined on anatomical MRI. These structural brain networks are symmetric by definition. Characterized using graph theory, some brain network properties are altered in certain disorders, such as bipolar illness [1, 2], body dysmorphic disorder [3], Alzheimer's disease [4], and even HIV/AIDS [5]. Large population studies, such as ADNI [6] and ENIGMA [7], are increasingly prevalent as they offer increased power to evaluate risk factors and biomarkers for diseases and detect genetic associations with brain measures.

Some studies have identified genetic effects on brain networks [8-10]. Jahanshad et al. [8] used a genome-wide association scan (GWAS) to screen brain connectivity matrices suggesting that common variants in the *SPON1* gene may influence anatomical networks. Candidate gene studies (e.g., [10]) have suggested lower global efficiency of the brain network in people carrying a variant in the Disrupted-in-Schizophrenia-1 (*DISC1*) gene, although these reports await replication.

However, dozens of tractography algorithms have been developed [11-17] yielding very different brain networks. We previously found no detectable differences in performance when classifying Alzheimer's Disease based on brain networks computed from nine tractography algorithms [18], but the choice of tractography algorithm may well affect genetic studies. Prior to embarking on large-scale GWAS studies of brain networks, here we evaluated nine different tractography methods with four different normalization approaches. We computed brain networks using each tractography algorithm and normalized each network using each normalization method. 10 network measures were extracted from each normalized network based on graph theory analysis. We addressed two questions: (1) Which normalization method leads to the least variation (i.e., greatest consistency) among different tractography algorithms; and (2) which network measures show greatest heritability, to prioritize or rank them for future in-depth genetic analyses.

2. METHODS

2.1 Participant Demographics and Imaging

DTI data from 853 young healthy adults were analyzed (**Table 1** shows their demographics). Each participant was scanned with 3D T1-weighted anatomical brain MRI and diffusion-weighted imaging (DWI) on a 4T Siemens Bruker Medspec MRI scanner. T1-weighted images were acquired with an inversion recovery rapid gradient echo sequence, with TI/TR/TE= 700/1500/3.35 ms; flip angle, 8°; slice thickness, 0.9 mm. Diffusion MRI was acquired using single-shot echo planar imaging with a twice-refocused spin echo sequence to reduce eddy-current induced distortions. Acquisition parameters were: 23 cm FOV, TE/TR 92.3/8250 ms. 105 images were acquired per subject: 11 with no diffusion sensitization (i.e., T2-weighted b_0 images) and 94 diffusion-weighted (DW) images (b=1159 s/mm^2) with gradient directions evenly distributed on the hemisphere. Total scan time was 14.5 minutes.

Table 1. Cohort Demographics.

	N	Age	Sex
Monozygotic twins (MZ)	228	22.38±2.74 y	72M
Dizygotic twins (DZ)	320	22.22±2.55 y	127M
Siblings	305	23.56±2.99 y	108M
Total	853	22.74±2.83 y	306M

2.2 Data Preprocessing

Non-brain regions were automatically removed from each T1-weighted image, and from a b0 image from the DWI dataset, using the *bet* function in FSL (http://fsl.fmrib.ox.ac.uk). A neuroanatomical expert manually refined all brain extractions. We corrected eddy current distortion in DWI scans using FSL's *eddy_correct* function. All T1-weighted scans were linearly aligned using FSL (with 9 DOF) to a common space. For each subject, the 11 eddy-corrected b_0 images were averaged, linearly aligned to the corresponding T1 image and elastically registered to the structural scan using a mutual information cost function to compensate for EPI-induced susceptibility artifacts. The resultant deformation field was applied to the other DWIs. Based on the registered DWIs, we computed whole-brain tractography with a wide variety of deterministic and probabilistic tracking algorithms that used tensor or full ODF-based models of diffusion.

2.3 Whole Brain Tractography

Among the deterministic methods were four tensor-based deterministic algorithms: FACT [12], the 2nd-order Runge-Kutta (RK2) method [11], the tensorline (TL) [13] and interpolated streamline (SL) methods [14] and two deterministic tractography algorithms based on 4th order spherical harmonic derived orientation distribution functions (ODFs) - FACT and RK2. We also tested three probabilistic

approaches: one was "ball-and-stick model based probabilistic tracking" (*Probtrackx*) from the FSL toolbox [15]; the other two were based on ODFs represented by 4th order spherical harmonic series: the Hough voting method [16] and the Probabilistic Index of Connectivity (PICo) method [17].

All deterministic tracking approaches were conducted with the Diffusion Toolkit (http://trackvis.org/dtk/). Fiber tracking was restricted to regions where fractional anisotropy (FA) ≥ 0.2 to avoid gray matter and cerebrospinal fluid; fiber paths were stopped if the fiber direction encountered a sharp turn (with a critical angle threshold $\geq$ 30°). Sharp "right-angle" turns may be biologically possible in some cases [19], but allowing right-angle turns in tractography would create large numbers of false positive pathways at fiber crossings.

Probtrackx was performed after *Bedpostx* was applied. *Bedpostx* stands for Bayesian Estimation of Diffusion Parameters Obtained using Sampling Techniques [15]. In our study, up to 3 fibers were modeled per voxel. Once Bedpostx had been run, we chose all voxels with FA$\geq$0.2 as the seeds. Following Bedpostx, Probtrackx was run on each individual seed voxel. Probtrackx repeatedly samples from the voxel-wise principal diffusion direction calculated in Bedpostx, creating a new streamline at each iteration. This builds a distribution on the likely tract location and path, given the data. A value of 1000 iterations was chosen to ensure convergence of the Markov chains, from which the posterior distributions of the local estimate of the fiber orientation distribution were sampled.

The Hough voting method was performed with code provided by the authors [16]. ODFs at each voxel were computed using the normalized and dimensionless constant solid angle ODF estimator, derived for Q-ball imaging (QBI) in [20]. Tractography was performed by probabilistically seeding voxels with a prior probability based on the FA value (FA$\geq$0.2). All curves passing through a seed point receive a score estimating the probability of the existence of the fiber, computed from the ODFs. Then a Hough transform voting process was adopted to determine the best fitting curves through each point. Hough probabilistic tractography optimizes the fiber pathway globally, so there is no explicit upper limit on the number of detectable crossing fibers although the data angular resolution will limit this in practice.

PICo was conducted with Camino (http://cmic.cs.ucl.ac.uk/camino/). Seed points were chosen at those voxels with FA $\geq$ 0.2. ODFs were estimated using 4th order Spherical Harmonics and a maximum of 3 local ODF maxima (where fibers mix or cross) were set to be detected at each voxel. Then, a probability density function (PDF) profile can be produced from the derived local ODF maxima. Monte Carlo simulation was used to generate fibers emanating from seed points inside the entire brain. Streamline fiber tracking followed the voxel-wise PDF

profile with the Euler interpolation method, for 10 iterations per each seed point. The maximum fiber turning angle was set to 30°/voxel. Tracing stopped at any voxel whose FA was less than 0.2. This approach generates many more fibers than other methods used in this study.

2.4 Brain Network Computing and Normalization

34 cortical regions of interest (ROI) per hemisphere, listed in [21], were automatically extracted from all aligned T1-weighted scans with FreeSurfer (http://surfer.nmr.mgh.harvard.edu). To ensure tracts would intersect cortical labeled boundaries, we dilated labels with an isotropic box kernel of size 5×5×5 voxels. For each ROI pair, the number of fibers connecting them was determined from the tractography. A fiber was considered to connect two ROIs if it intersected both ROIs. This process was repeated for all ROI pairs, to compute a 68x68 whole brain fiber connectivity matrix. This matrix (M_0) is symmetric, by definition, and the diagonal elements represent the total number of fibers originating from each ROI. Since Probtrackx can output the brain network directly, the results from all other tractography algorithms except Probtrackx were analyzed using the above procedures to generate brain network. We then defined four ways to normalize these brain networks (**Table 2**).

<p align="center">Table 2. Matrix Normalization</p>

	Equation
Raw	$M1 = M_0 \circ (1-E)$
MaxNorm	$M2 = M1 \circ (1/max(M1))$
SumNorm	$M3 = M1 \circ (1/sum(M1))$
IndNorm	$M4(i,j) = \dfrac{M_0(i,j) \circ (1-E)}{[M_0(i,i) + M_0(j,j) - M_0(i,j)]}$
M_0 is the initial computed matrix; E is the unit matrix; ∘ is the Hadamard product; max() is the maximum value of all matrix elements; sum() is summation of all matrix elements; (i,j) is the element (i,j) in the matrix. M1-M4 are four normalized matrices.	

2.5. Network measures

After normalization, M1-M4 were analyzed using graph theory. Nine network global measures were calculated including Mean Clustering Coefficient (MCC), Transitivity (TS), Characteristic Path Length (CPL), Density (DS), Degree (DG), Global Efficiency (GLOB), Strength (ST), Diversity (DV) and Small-Worldness (SW), using the brain connectivity toolbox (BCT) [22]. We used weighted versions of these 9 measures. Definitions and mathematical equations may be found at the BCT toolbox website (https://sites.google.com/site/bctnet/).

2.6. Statistical Analysis

For each network measure listed in section 2.5, we used generalized linear regression (GLR) to remove statistical effects of age, sex and total brain volume (TBV). The resultant residue (RR) was used for the following two analyses.

Our first aim was to find which normalization technique would minimize the variations among different tractography algorithms, i.e. yield most consistent networks across methods. So we ran one-way ANOVA on four sets of normalized matrices using all 853 subjects. Each group consists of 853 values. We first computed each subject's variability across the nine tractography algorithms, defined as Q=abs(SD/mean), in which abs is absolute value, SD is the standard deviation of RR_i (i=1-9) and the mean is the mean value of RR_i (i=1-9). RR_i is the residual network corresponding to the i-th tractography algorithm. We repeated this process nine times for the nine network measures in section 2.5.

Second, based on the "optimal" normalization technique, we aimed to find which tractography algorithm and which network measures showed evidence of heritability (genetic influence). So for each network measure from 114 pairs of MZ and 160 pairs of DZ twins, we fitted a structural equation model (SEM) to estimate to what extent the variance in each measure was attributable to additive genetic, *A*, common environment, *C*, and unique environment/measurement error, *E* (please refer to [23] for model details). MZ twins raised in a family share 100% of their genes, as well as a shared environment. Any differences arising between them in these circumstances are random (unique). The correlation between identical twins provides an estimate of *A + C*. DZ twins also share *C*, but share on average only 50% of their genes: so the correlation between fraternal twins is a direct estimate of ½*A+C*. Therefore, the additive genetic component of variance, a^2, is approximately twice the difference between identical and fraternal twin correlations: the additive genetic effect (Falconer's formula) [24]. Measures with lower a^2 values tend to be less promising candidates for further genetic analysis.

3. RESULTS AND DISCUSSIONS

3.1 Normalization Effects

Figure 1 shows One-Way ANOVA results on variability (*Q*) for network measures in the four normalization groups across the cohort described in **section 2.6**. Only three measures (MCC, DV and TS) show significant differences in consistency that depends on the normalization method in One-Way ANOVA (*P= P*=2.5×10^{-3}, 7.69×10^{-3} and 5.82×10^{-5} respectively). As only the IndNorm method gave consistently significant smaller mean variability (i.e., greater consistency) for these three network measures and there are no group differences in *Q* among four normalization

methods for the other six network measures, we chose the IndNorm method for later analysis.
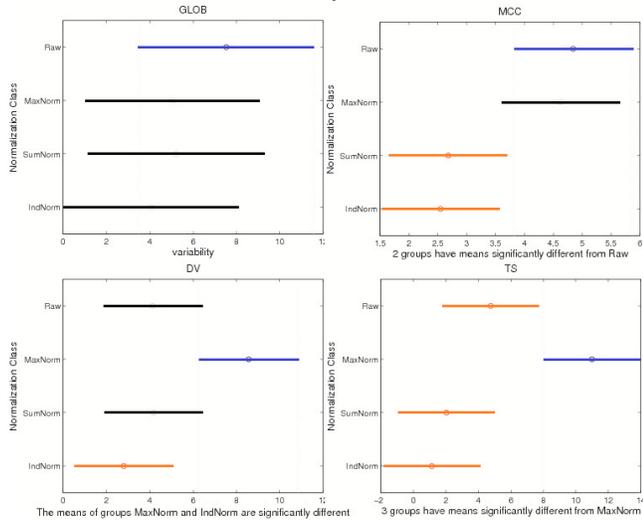

Figure 1. One-Way ANOVA results for network measures. The y-axis shows the type of normalization used, and the x-axis is variability (Q) and its 95% confidence interval (CI) across the cohort described in **Section 2.6**. No CI overlap suggests significant differences between normalization methods. Different colors (*blue and red*) show pairs of methods with significant differences. We show GLOB as one example where there was no detectable difference in mean variability across the four normalization methods. For the network metrics MCC, DV and TS, there are significant differences among the four normalization methods - with $P=2.5 \times 10^{-3}$, 7.69×10^{-3} and 5.82×10^{-5} respectively in a one-way ANOVA.

3.2 Heritability statistic

Based on the above results, we computed ACE-based heritability statistics for the IndNorm group only. **Figure 2** shows the heritability statistic results (a^2 values with $P < 0.05$) for all network measures and for nine tractography algorithms. Our results indicated most A values do not differ detectably from zero, so those measures may not be suitable for further genetic studies. Five measures (including Tensor-TL derived TS, Probtrackx-derived GLOB, ST, DV and Hough-derived CPL) are highlighted in **Figure 2. Table 3** summarizes the ACE outputs for these five measures.

From **Table 3**, if Bonferroni correction is adopted to correct for multiple comparisons, our results still showed that Probtrackx-derived GLOB and ST have significant $\mathbf{a^2}$ values (P_A less than $0.05/9/9 \approx 6.2E-04$). Probabilistic tractography algorithms with global optimization (such as Probtrackx and Hough) may yield higher heritability statistics for genetic studies than other "greedy" types of tractography algorithms (such as FACT) which process small neighborhoods at each step. Furthermore, probtrackx-derived GLOB and ST have significant (and large) $\mathbf{a^2}$ values (*red colors* in **Table 3**). For these measures, genetic factors may account for over 50% of the measured variance among individuals.
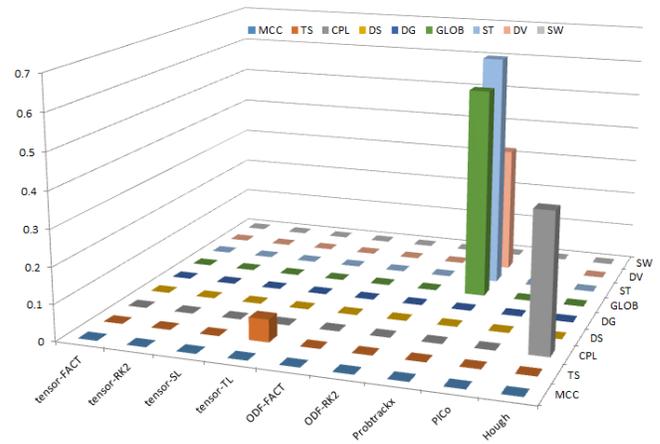

Figure 2. SEM heritability statistic results (a^2 values) for all network measures and for all tractography algorithms, when using IndNorm as normalization method. Only Tensor-TL derived TS, Probtrackx-derived GLOB, ST, DV and Hough-derived CPL have a^2 values significantly larger than 0 (with P value<0.05). Most of other measures have zero values.

Table 3. Summary of ACE output for the five highlighted measures. 1: Tensor-TL derived TS; 2-4 ： Probtrackx-derived GLOB, ST and DV; 5: Hough-derived CPL. P_{ACE} represents how well the ACE model fits; the *larger* this value is, the better the ACE model fits. P_A is the probability associated with the A term in ACE model.

Index	P_{ACE}	P_A	a^2 (%)	c^2 (%)	e^2(%)
1	0.60	8.51E-03	6.18	0	93.82
2	0.28	5.88E-05	58.11	0	41.89
3	0.11	1.13E-06	64.65	0	35.35
4	0.17	3.15E-02	35.18	0	64.82
5	0.99	4.6E-02	38.01	15.49	46.50

4. CONCLUSIONS

In our study, we the first used an IndNorm normalization technique to increase the consistent among network measures computed from 9 different tractography algorithms. Probabilistic tractography algorithms with global optimization generated measures in which a greater proportion of the variance was attributable to genetic differences among individuals. Probtrackx-derived GLOB and ST were two measures for which genetic factors explained over half of the overall variance across individuals. This suggests the value of further genetic association analysis, at least for these measures. Also in current study, we only investigated typical global network measures, which are averages computed from local network measures. Future work will also assess local network measures.

5. REFERENCES

[1] Leow, A., et al., *Impaired Inter-Hemispheric Integration in Bipolar Disorder Revealed with Brain Network Analyses.* Biological Psychiatry. 73(2):183:193. 2013.

[2] GadElkarim, J., et al., *A Framework for Quantifying Node-Level Community Structure Group Differences in Brain Connectivity Networks.* Medical Image Computing and Computer-Assisted Intervention–MICCAI 2012: p. 196-203. 2012.

[3] Arienzo, D., et al., *Abnormal brain network organization in body dysmorphic disorder.* Neuropsychopharmacology, **38**(6): p. 1130-9.2013.

[4] Nir, T., et al., *Small World Network Measures Predict White Matter Degeneration in Patients with Early-Stage Mild Cognitive Impairment.* Proc IEEE Int Symp Biomed Imaging: p. 1405-1408.2012.

[5] Jahanshad, N., et al., *Disrupted brain networks in the aging HIV+* population. Brain Connect. 2(6):335-344. 2012.

[6] Mueller, S.G., et al., *Ways toward an early diagnosis in Alzheimer's disease: the Alzheimer's Disease Neuroimaging Initiative (ADNI).* Alzheimers Dement, **1**(1): p. 55-66.2005.

[7] Stein, J.L., et al., *Identification of common variants associated with human hippocampal and intracranial volumes.* Nat Genet, **44**(5): p. 552-61. 2012.

[8] Jahanshad, N., et al., *Genome-wide scan of healthy human* connectome *discovers SPON1 gene variant influencing dementia severity.* Proc Natl Acad Sci U S A, **110**(12): p. 4768-73. 2013.

[9] Thompson, P.M., et al., *Genetics of the connectome.* Neuroimage, **80**: p. 475-88. 2013.

[10] Li, Y., et al., *Less efficient information transfer in Cys-allele carriers of DISC1: a brain network study based on* diffusion *MRI.* Cereb Cortex, **23**(7): p. 1715-23.2013.

[11] Basser, P.J., et al., *In vivo fiber tractography using DT-MRI data.* Magn Reson Med, **44**(4): p. 625-32. 2000.

[12] Mori, S., et al., *Three-dimensional tracking of axonal projections in the brain by magnetic resonance imaging.* Ann Neurol, **45**(2): p. 265-9. 1999.

[13] Lazar, M., et al., *White matter tractography using diffusion tensor deflection.* Hum Brain Mapp, **18**(4): p. 306-21.2003.

[14] Conturo, T.E., et al., *Tracking neuronal fiber pathways in the* living *human brain.* Proc Natl Acad Sci U S A, **96**(18): p. 10422-7.1999.

[15] Behrens, T.E., et al., *Probabilistic diffusion tractography with* multiple *fibre orientations: What can we gain?* Neuroimage, **34**(1): p. 144-55.2007.

[16] Aganj, I., et al., *A Hough transform global probabilistic* approach *to multiple-subject diffusion MRI tractography.* Med Image Anal, **15**(4): p. 414-25.2011.

[17] Parker, G.J., H.A. Haroon, and C.A. Wheeler-Kingshott, *A framework for a streamline-based probabilistic index of connectivity (PICo) using a structural interpretation of MRI diffusion measurements.* J Magn Reson Imaging, **18**(2): p. 242-54. 2003.

[18] Zhan, L., et al., *Comparison of 9 Tractography Algorithms for Detecting Abnormal Structural Brain Networks in Alzheimer's Disease.* Submitted to PLOS ONE. 2014.

[19] Wedeen, V.J., et al., *The geometric structure of the brain fiber pathways.* Science, **335**(6076): p. 1628-34.2012.

[20] Aganj, I., et al., *Reconstruction of the orientation distribution function in single- and multiple-shell q-ball imaging within constant solid angle.* Magn Reson Med, **64**(2): p. 554-66. 2010.

[21] Desikan, R.S., et al., *An automated labeling system for subdividing the human cerebral cortex on MRI scans into gyral based regions of interest.* Neuroimage, **31**(3): p. 968-80. 2006.

[22] Rubinov, M. and Sporns, O., *Complex network measures of brain connectivity: uses and interpretations.* Neuroimage, **52**(3): p. 1059-69. 2010.

[23] Neale, M., Baker, S., Xie, G., Maes, H., Mx: Statistical *modeling*, 6th ed. (2002).

[24] McGraw, K.O. and S.P. Wong, *Forming inferences about some intraclass correlation coefficients.* Psychological Methods, **1**(1): p. 30-46. 1996.